A porphyrin-based metal-organic framework with highly efficient adsorption and photocatalytic degradation of organic dyes

Xiong-Hai Chen,[a] *Yun-Shi Zhang,*[a] *Wen-Bin Li,*[a] *Xiu-Wen Guan,*[a] *Jia-Wen Ye,*[a] *Ling Chen,*[a] *Hai-Ping Wang,*[a] *Jie Bai,*[b] *Zong-Wen Mo,**[a] *and Xiao-Ming Chen*[a,c]

[a] School of Biotechnology and Health Sciences, Wuyi University, Jiangmen, Guangdong 529000, PR China.

[b] Analysis and Test Center, Guangdong University of Technology, Guangzhou 510275, China.

[c] MOE Key Laboratory of Bioinorganic and Synthetic Chemistry, School of Chemistry, Sun Yat-Sen University, Guangzhou 510275, China.

*Email: wyuchemmzw@126.com

Calculation of capacity.

The adsorption capacities at a given time and equilibrium are calculated as equation: (**1**)

$Q_e = V \cdot (C_0 - C_e) \cdot M/m$ (**1**)

where V is the volume of the dye solution, C_0, and C_e represent the concentration of dye solution at the initial and equilibrium time, respectively. m is the adsorbent mass of **1**.

Photocatalytic degradation of dyes of kinetics.

Dynamic analysis of the catalysis of dyes shows that the degradation of the dye is a first-order reaction, and the first-order model is expressed by equation (**2**, Langmuir–Hinshelwood model). The kinetic constant (k) reflects the speed of photodegradation.

$-\ln(C/C_0) = k \cdot t$ (**2**) The k value is the kinetic constant, and the slope of the linear plot.

Calculation of degradation efficiency.

The degradation efficiency of dyes is calculated using the following equation (**3**)

Degradation efficiency (%) = $(1 - C/C_0) \cdot 100\%$ (**3**)

C and C_0 represent the apparent and initial concentrations of dyes, respectively.

Adsorption kinetics study.

The pseudo-second/first-order model was used to fit the kinetic results. The related equation can be expressed as follows:

$t / Q_t = 1 / (k_1 Q_e^2) + t / Q_e$

$\ln(Q_e - Q_t) = \ln Q_e - k_2 t$

k_1 (g·mg^{-1} min^{-1}) is the rate constant of adsorption, which was calculated from the intercept/slope of t / Q_t vs t plot and k_2 (min^{-1}) was obtained from the slope of $\ln(Q_e - Q_t)$ vs t plot.

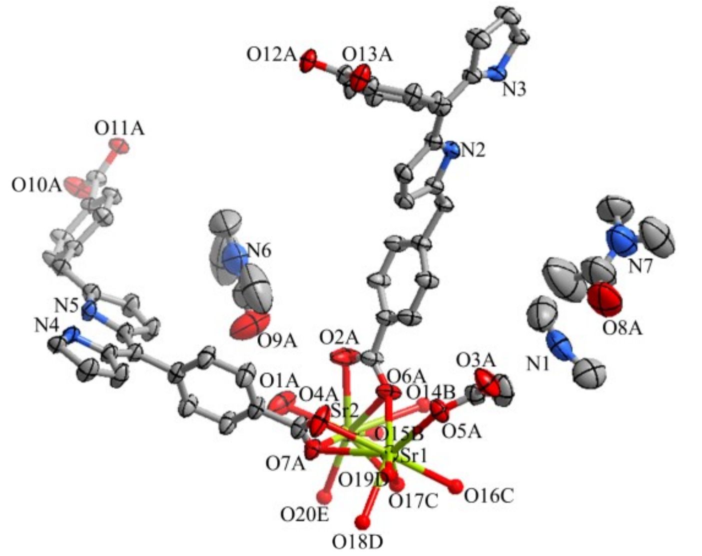

Fig. S1. Perspective view of the asymmetric unit of **1** (symmetry codes: A = 2-*x*, 2-*y*, 1-*z*; B = 3-*x*, 2-*y*, 1-*z*; C = 5/2+*x*, 5/2-*y*, 1/2+*z*; D = -1/2*x*, 5/2-*y*, 1/2+*z*; E = 1/2+*x*, 5/2-*y*, 1/2+*z*).

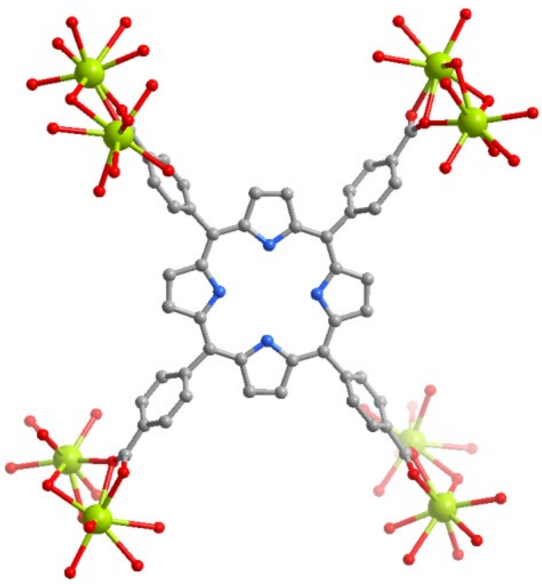

Fig. S2. The coordination mode of $TCPP^{4-}$ ligand in **1**.

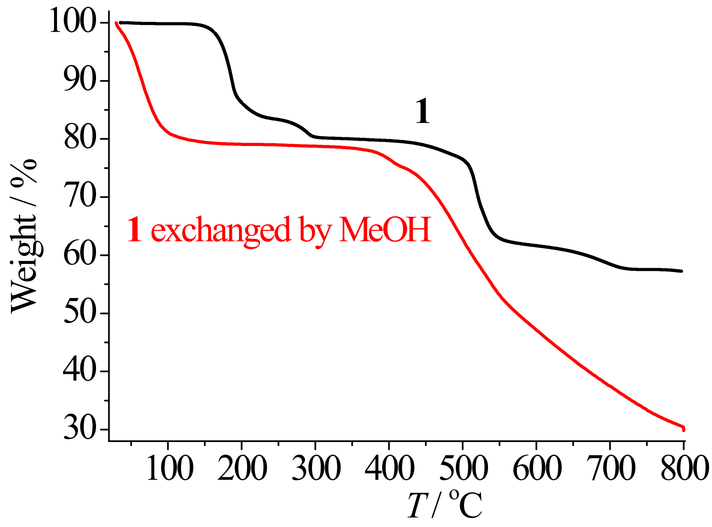

Fig. S3. The thermogravimetry curves of **1** and MeOH-exchanged **1**.

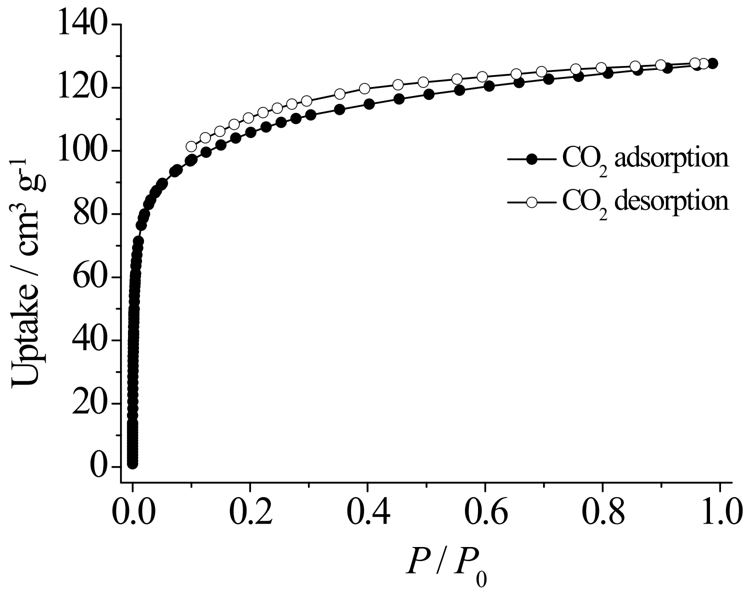

Fig. S4. CO_2 sorption isotherms for **1** at 195 K.

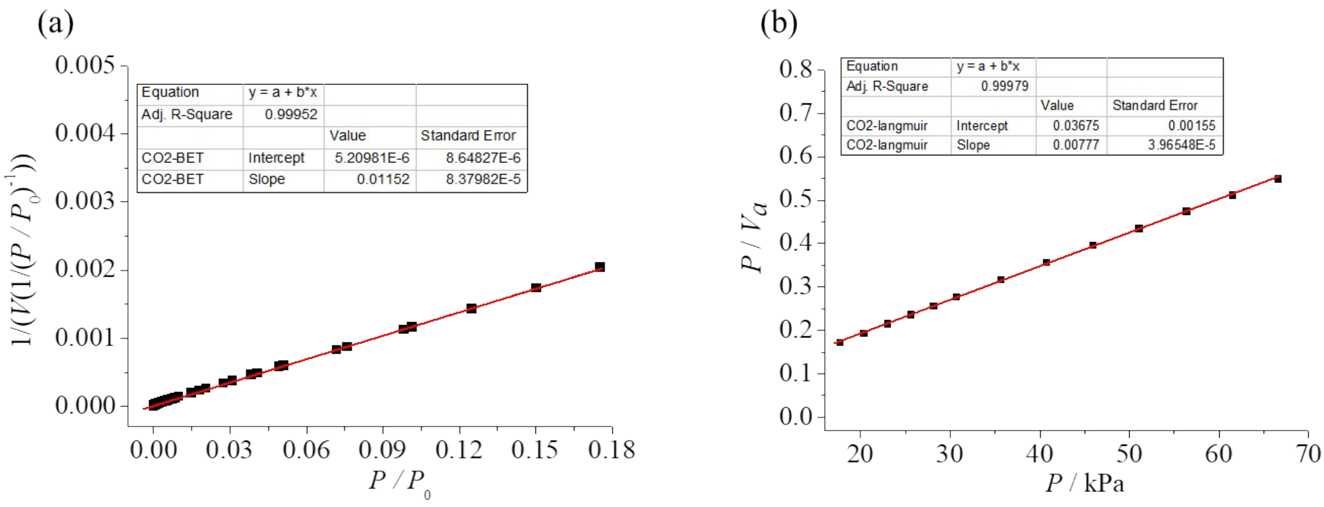

Fig. S5. (a) BET and (b) Langmuir fittings of the CO_2 adsorption isotherm for **1**.

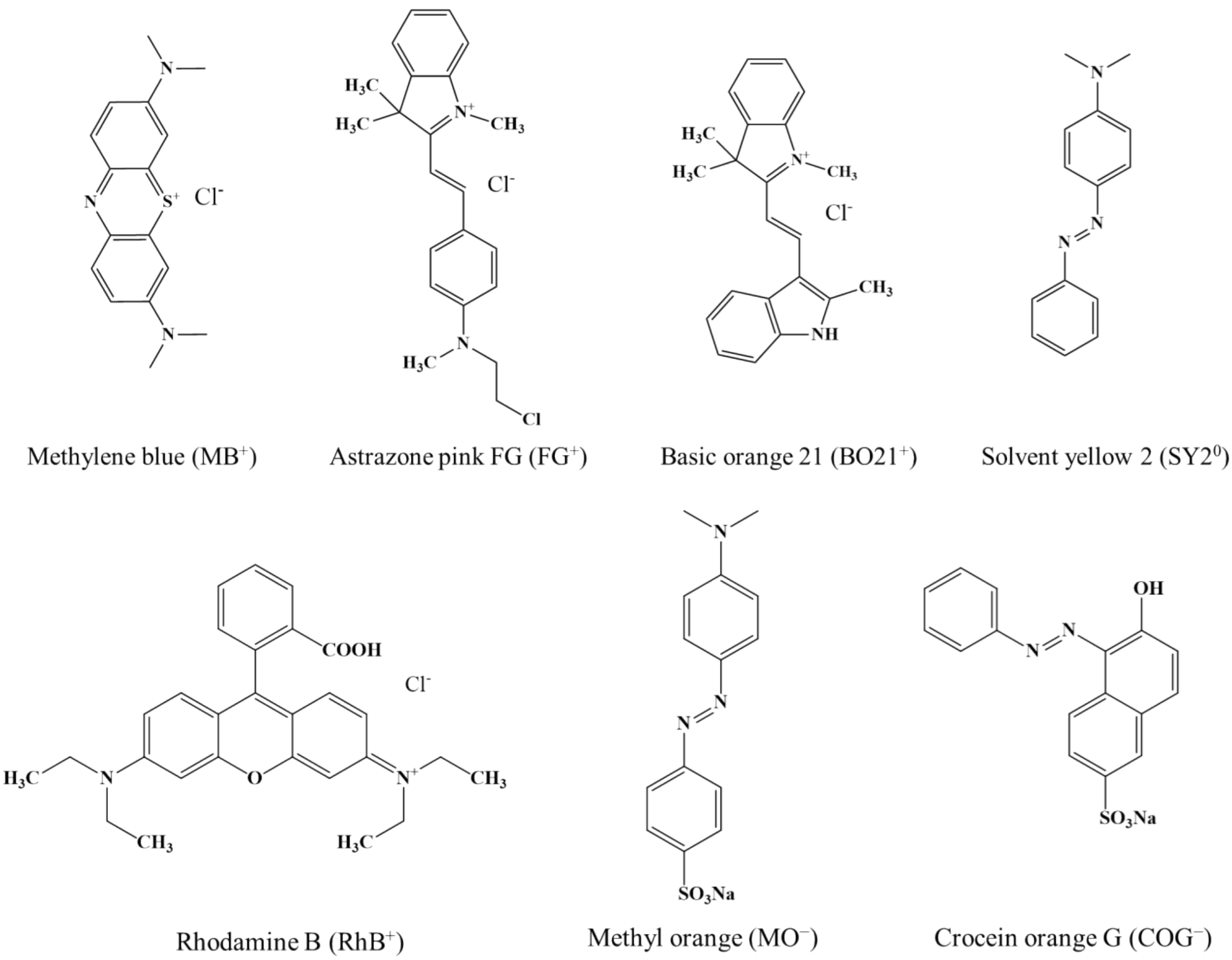

Fig. S6. Structures of the dye molecules.

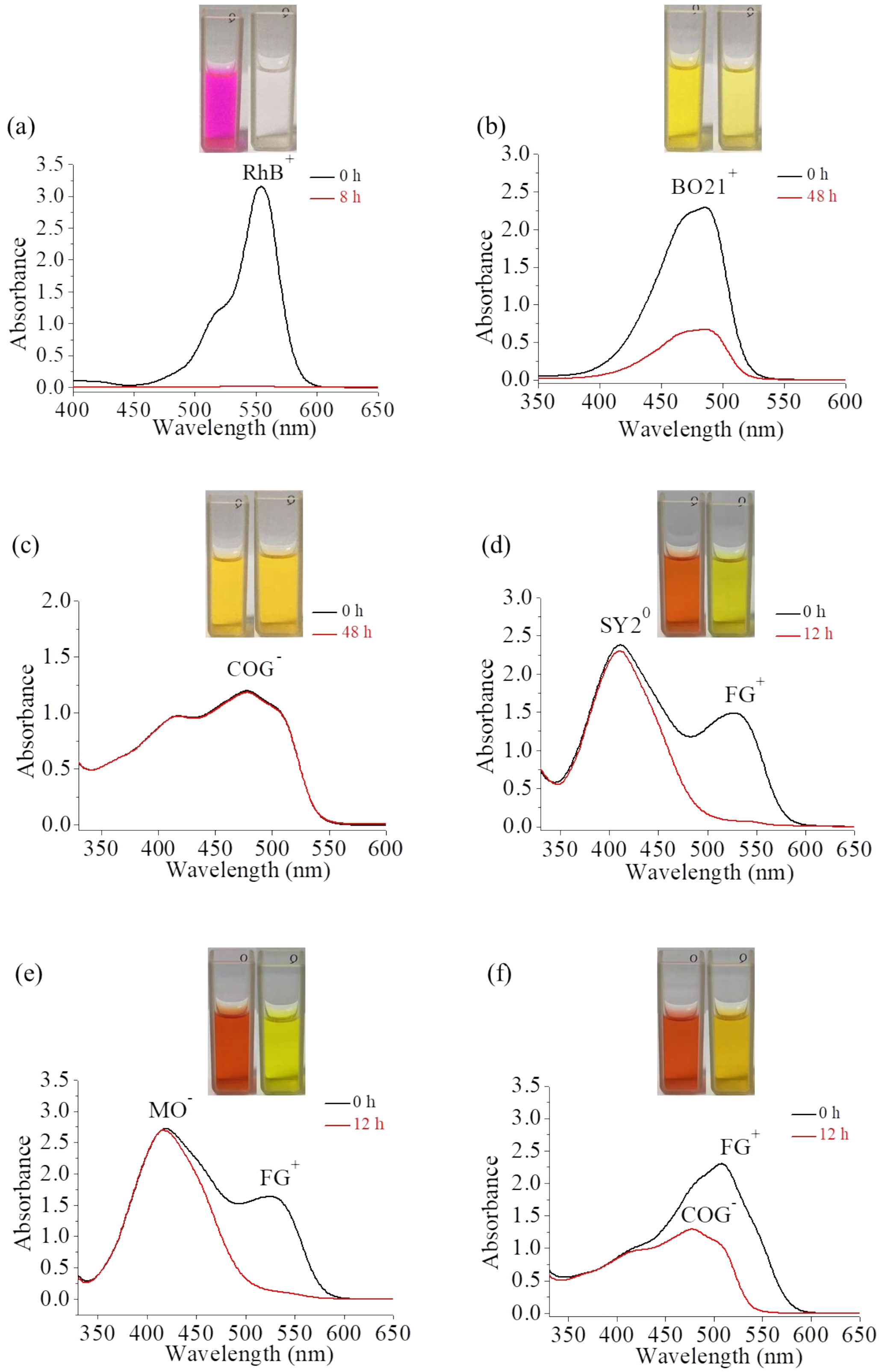

Fig. S7. UV-vis absorbance of (a) RhB^{+} (0.25 mmol L^{-1}), (b) $BO21^{+}$ (0.1 mmol L^{-1}), and (c) COG^{-} (0.1 mmol L^{-1}). Two-component dye adsorption of (d) $SY2^{0}$ and FG^{+}, (e) MO^{-} and FG^{+} and (f) COG^{-} and FG^{+} (0.1 mmol L^{-1} and 0.1 mmol L^{-1}). Inset: photographs showing visual colour changes of the dye solution.

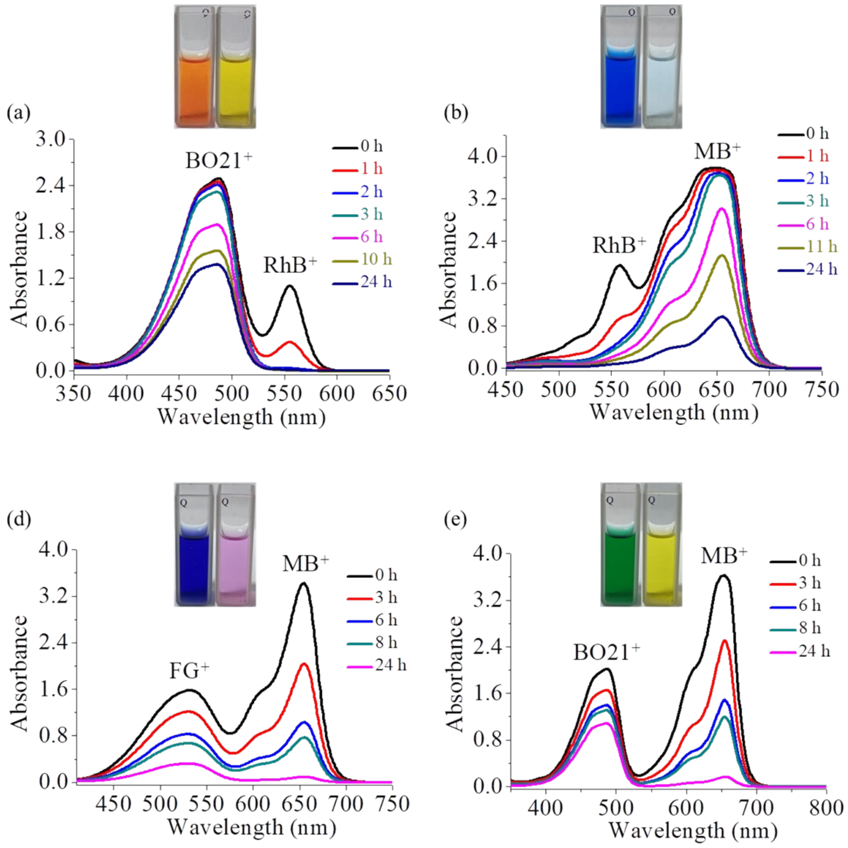

Fig. S8. Two-component dye adsorption of (a) RhB^+ and $BO21^+$, (b) RhB^+ and MB^+, (c) FG^+ and $BO21^+$, (d) FG^+ and MB^+ and (e) $BO21^+$ and MB^+ (0.1 mmol L^{-1} and 0.1 mmol L^{-1}).

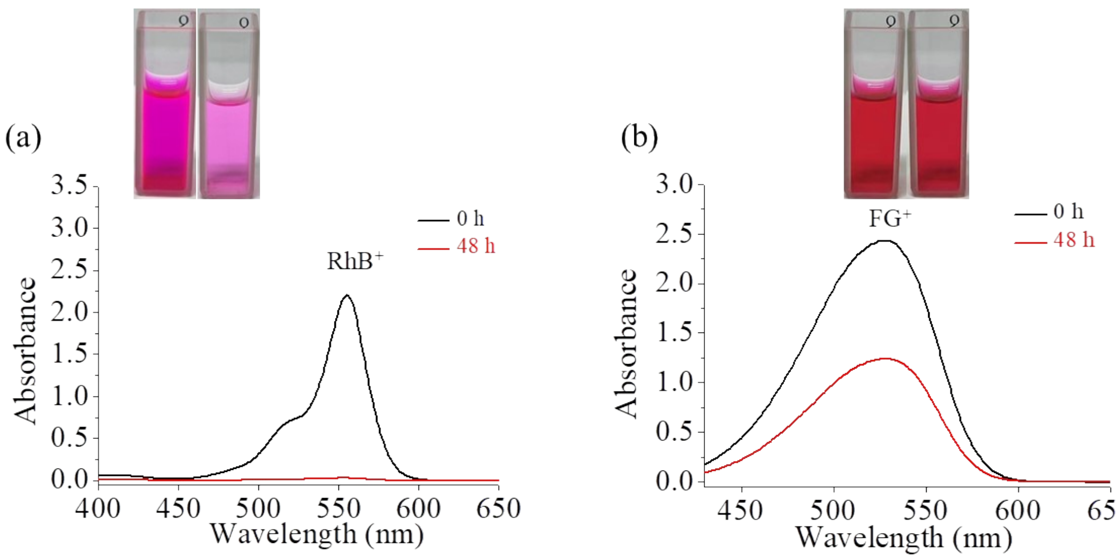

Fig. S9. UV−vis absorption spectra for dye adsorption with high concentration of (a) RhB^+ (1 mmol L^{-1}) and (b) FG^+ (0.6 mmol L^{-1}). Inset: photographs showing visual colour changes of the dye solution before and after adsorption experiment.

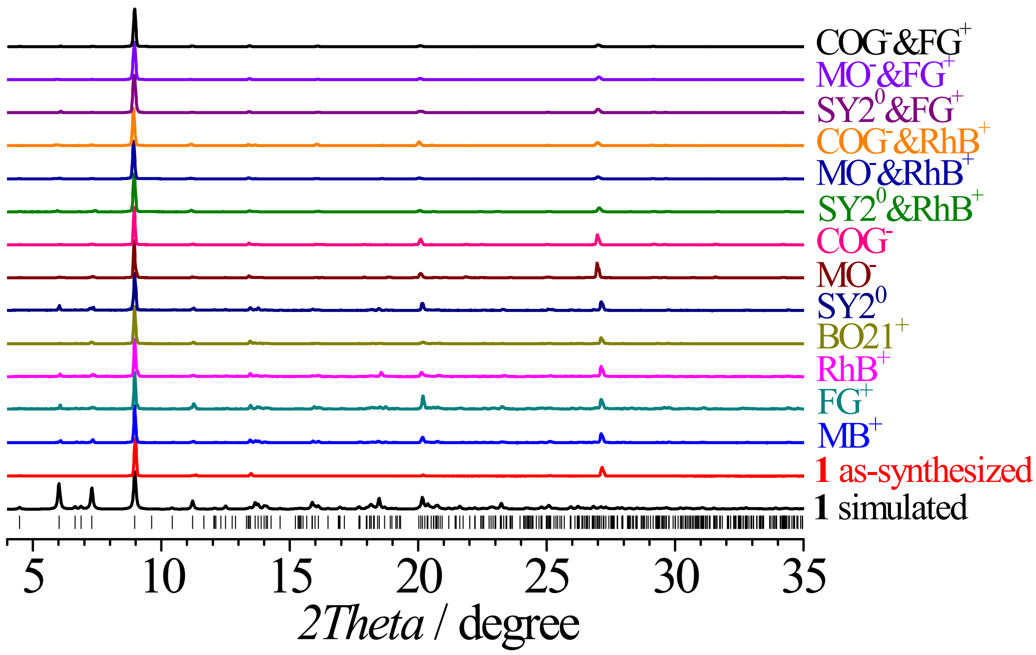

Fig. S10. PXRD patterns of **1** after dye exchange experiments.

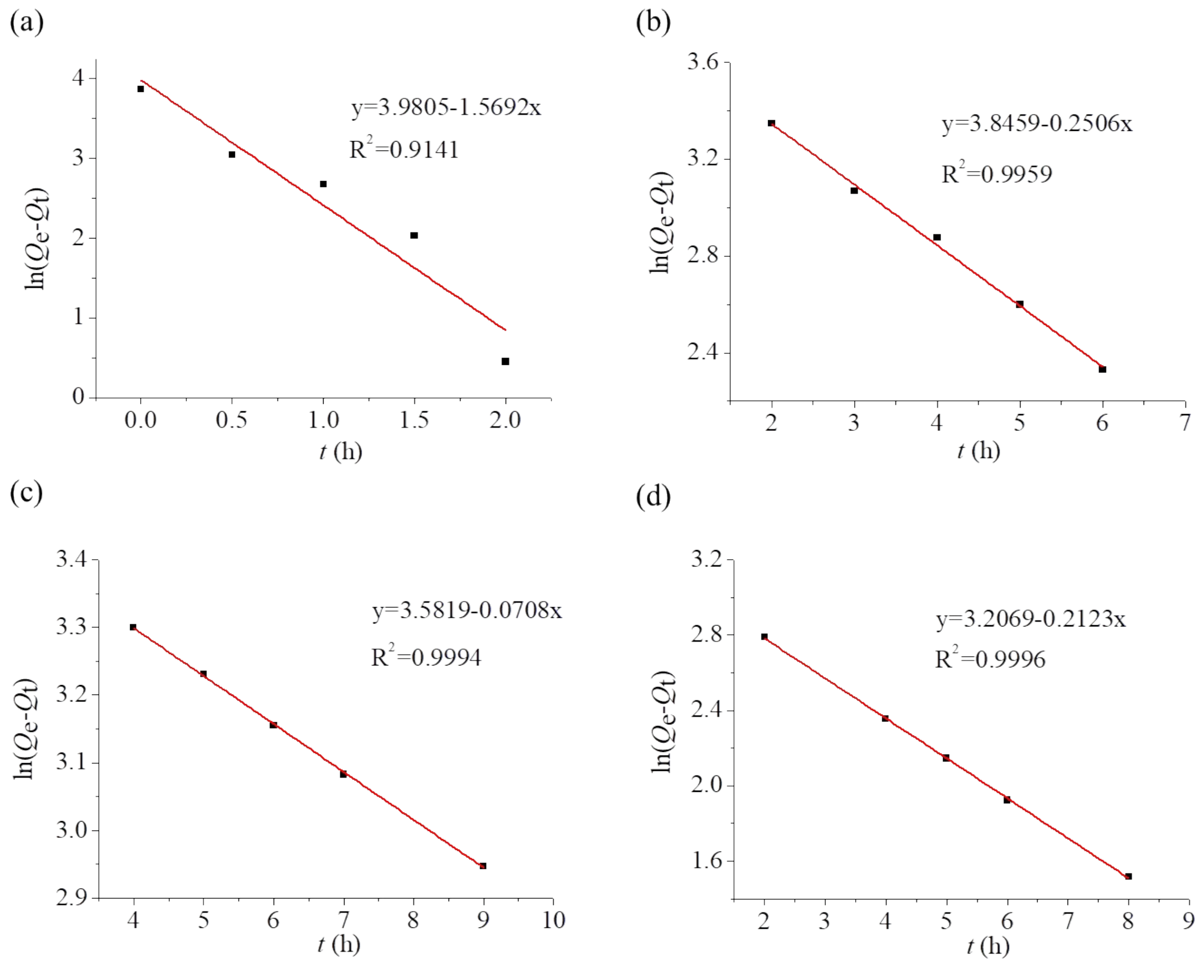

Figure S11. Plot of the pseudo-first-order kinetic model for (a) RhB^+, (b) FG^+, (c) $BO21^+$ and (d) MB^+.

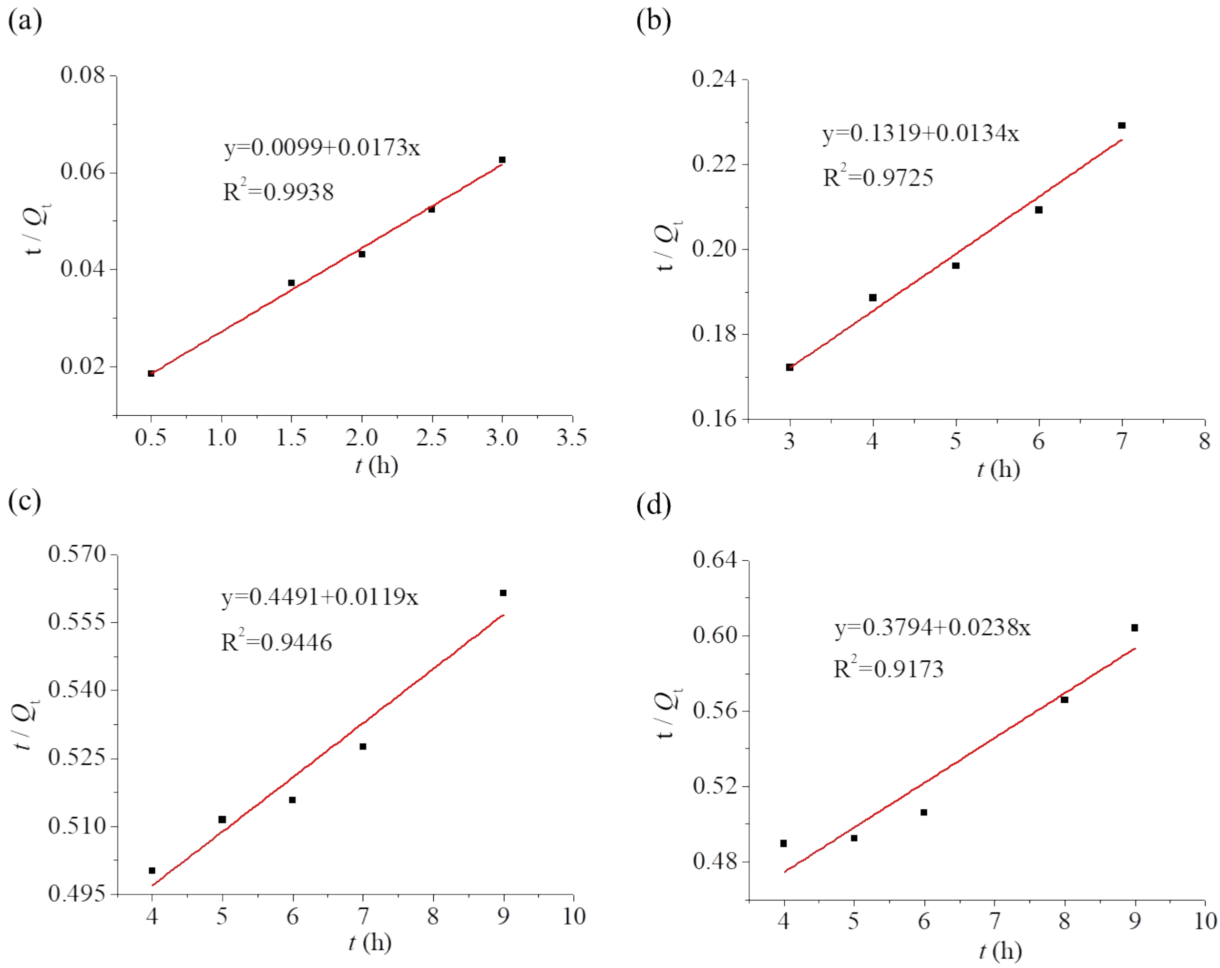

Figure S12. Plot of the pseudo-second-order kinetic model for (a) RhB^+, (b) FG^+, (c) $BO21^+$ and (d) MB^+.

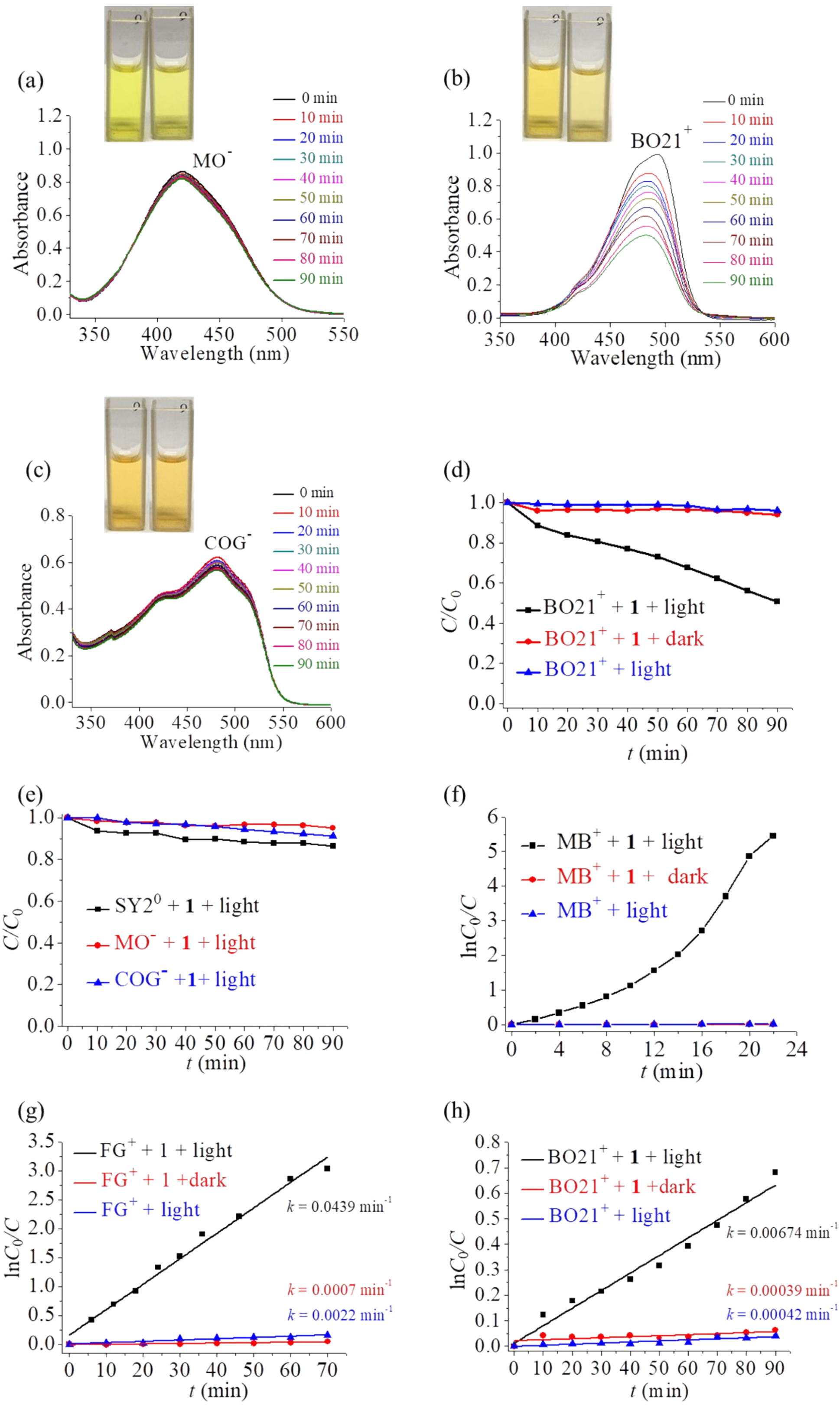

Fig. S13. UV-vis absorption spectra of (a) $BO21^+$, (b) MO^- and (c) COG^- recorded at various times during the photocatalytic process, photocatalytic oxidation performances of **1** for (d) $BO21^+$, (e) $SY2^0$, MO^- and COG^-. Plots of $\ln(C_0/C)$ with respect to time for (f) MB^+, (g) FG^+, and (h) $BO21^+$, providing apparent reaction rate constants (k).

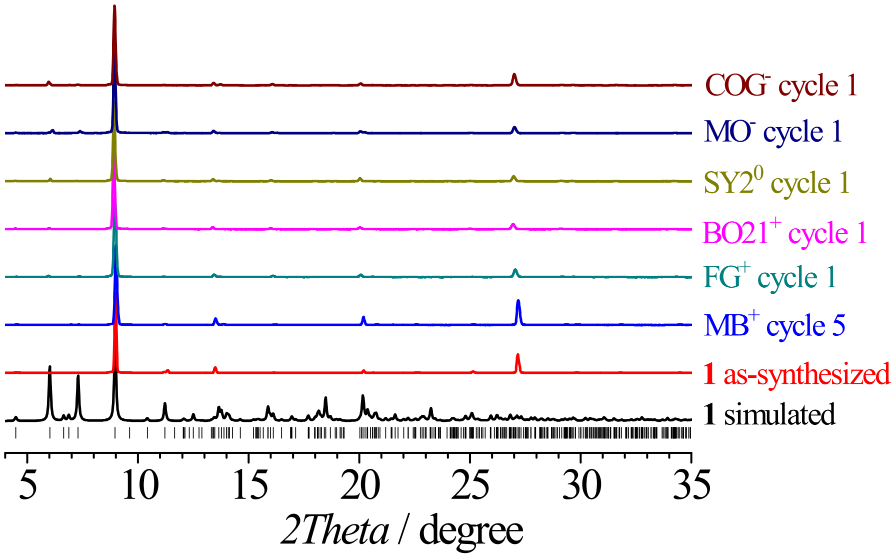

Fig. S14. PXRD patterns of **1** after photocatalytic experiments.

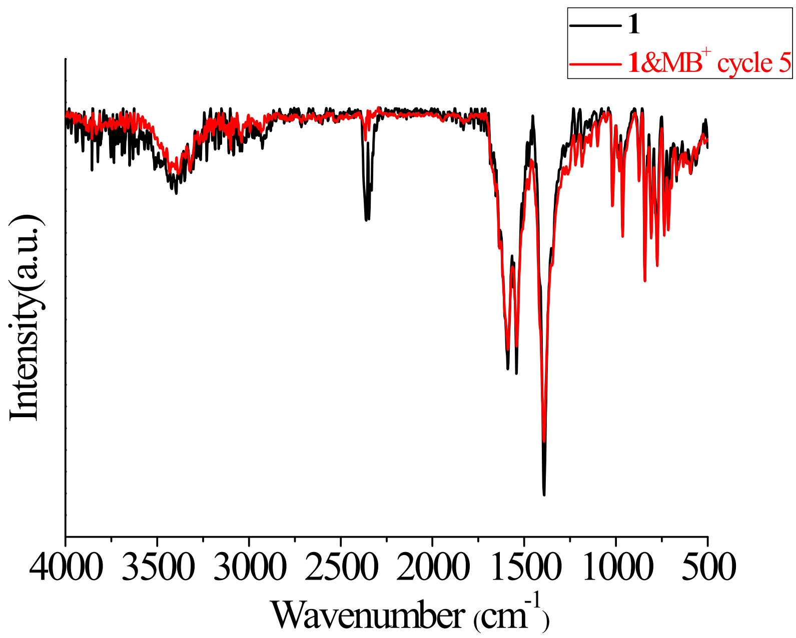

Fig. S15. Infrared spectra of **1** before and after photocatalytic experiments of five consecutive photocatalytic recycles for the degradation of MB^{+}.

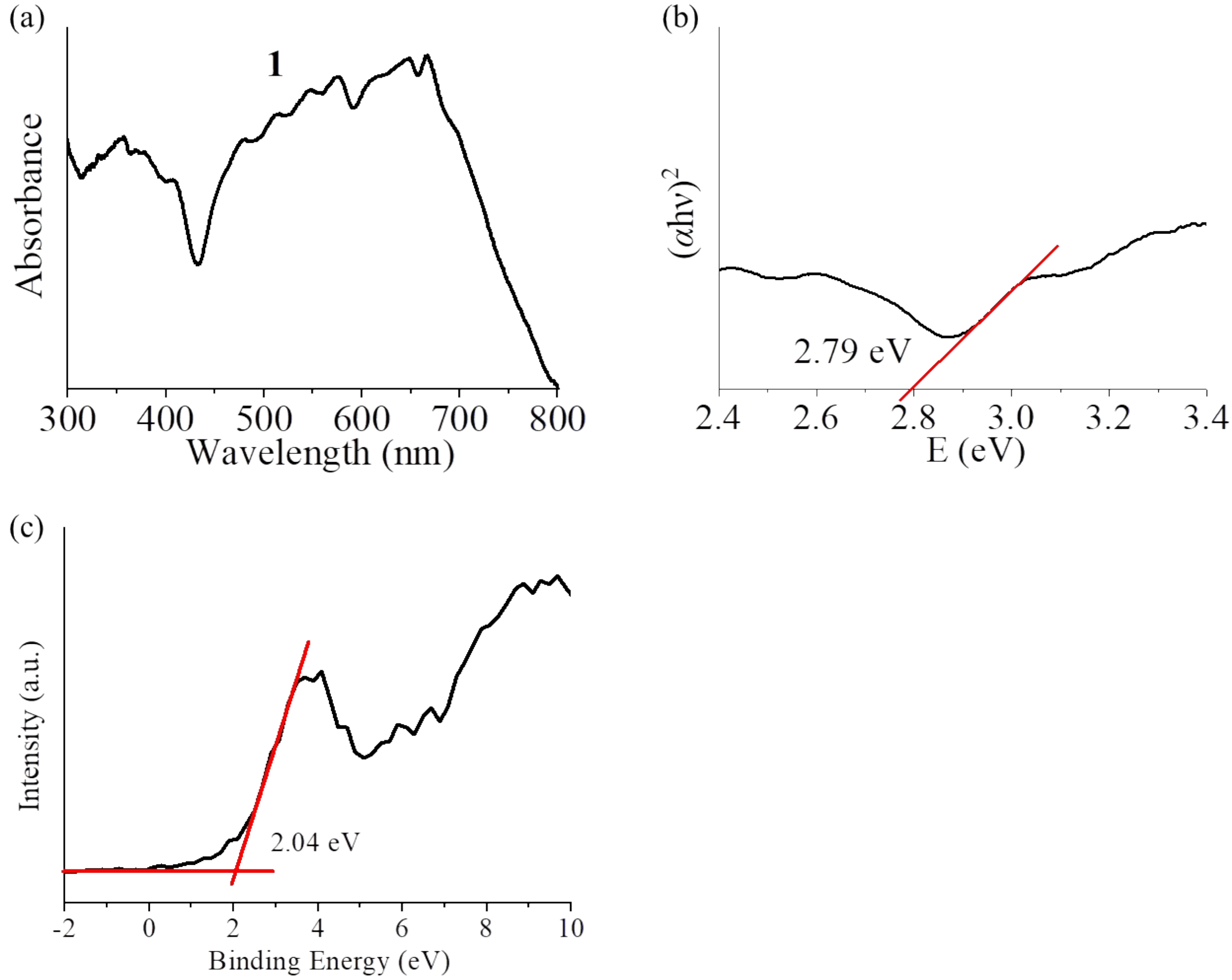

Fig. S16. (a) UV–vis diffuse reflectance spectrum (DRS) spectrum of **1**, (b) Tauc plot of the UV-vis DRS spectrum of **1** and (c) VB XPS diagram of **1**.

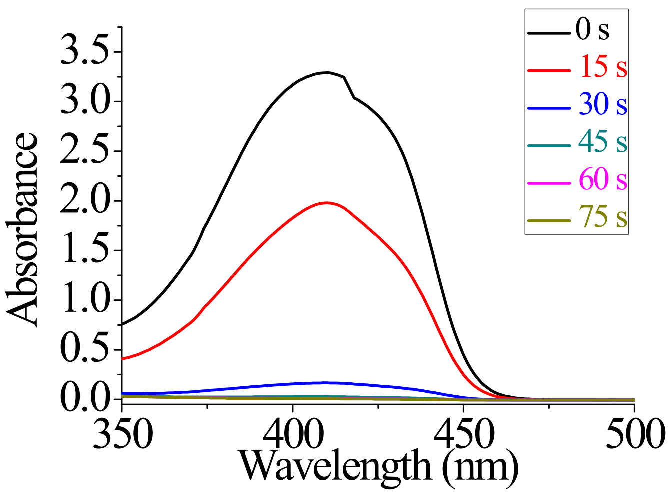

Fig. S17. Time evolution of the absorption spectra of DPBF under visible light irradiation.

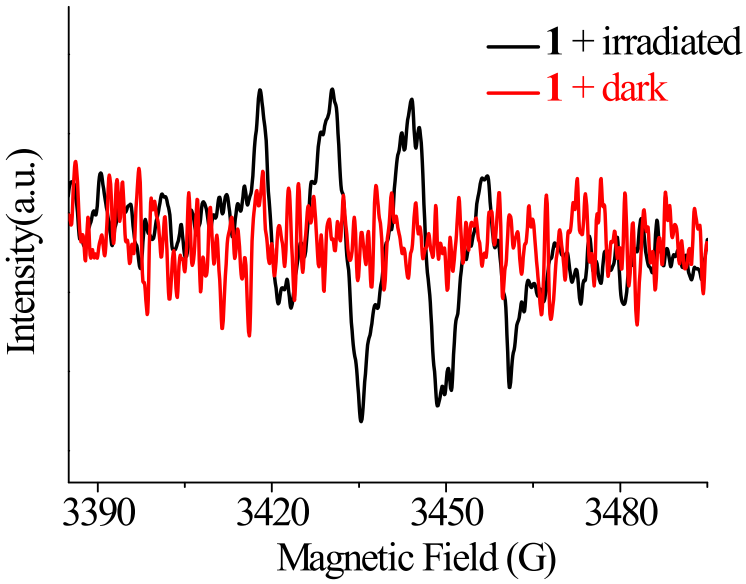

Fig. S18. DMPO/$\cdot O_2^-$ spin-trapping ESR spectra of **1** in methanol before and after irradiation.

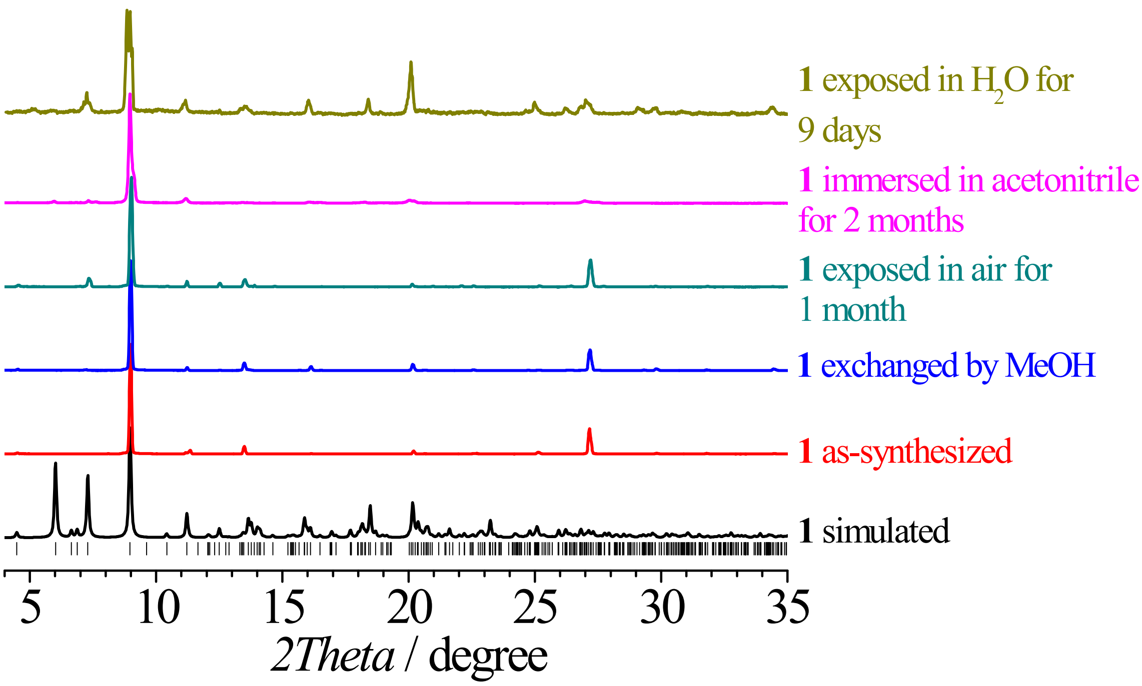

Fig. S19. PXRD patterns of **1** under different environments.

Table S1. Crystallographic data and structural refinement detail of **1**.

Complex	**1**
Formula	$C_{60}H_{57}N_7O_{13}Sr_2$
Formula weight	1259.36
Temperature (K)	298(2)
Crystal system	monoclinic
Space group	$P2_1/n$
a/Å	7.67080(4)
b/Å	26.58541(16)
c/Å	29.55061(17)
β/°	96.5378(5)
V/Å^3	5987.11(6)
Z	4
D_c /g cm^{-3}	1.397
reflns coll.	11011
unique reflns	12013
R_{int}	0.0423
R_1 $[I > 2\sigma(I)]^a$	0.0386
wR_2 $[I > 2\sigma(I)]^b$	0.1052
R_1 (all data)	0.0414
wR_2 (all data)	0.1073
GOF	1.028

$^a R_1 = \Sigma||F_o|-|F_c||/ \Sigma|F_o|$.

$^b wR_2 = \{\Sigma w[(F_o)^2-(F_c)^2]^2/ \Sigma w[(F_o)^2]^2\}^{1/2}$

Table S2. Comparison of RhB^+ adsorption capacities in MOFs.

Dyes	MOFs	Q_e (mg/g)	Ref
RhB^+	LIFM-WZ-3	141.5	1
	LIFM-WZ-4	61.8	2
	UPC-102-Zr	195	3
	NH_2-MOF-199	156	4
	JUL-liu 397	16	5
	MIL-100(Fe)	194.17	6
	SCNU-Z2	751.8	7
	CP1	24.36	8
	MOF-808(Zr)	166.7	9
	CPM-97-Fe	306	10
	1	**472.8**	**This work**

Table S3. Comparison of the photocatalytic degradation performances of MOFs on methylene blue (MB^+).

MOFs	Dye	Concentration and quantity (mg L^{-1})	Irradiation	Degradation Time (min)	Degradation Efficiency (%)	Ref
[Co_2(tkcomm)(tkiymm)]	MB^+	3.51	Vis (500 W)	300	50	11
MIL-53(Fe)	MB^+	140	Vis (500 W)	40	20	12
Fe_3O_4@MIL-100(Fe)	MB^+	40	Vis (500 W)	20	20	13
[Co_2(1,4-bdc)(ncp)$_2$]	MB^+	35.1	UV (375 W)	300	63	14
MIL-88A	MB^+	32	Vis (300 W)	20	100	15
g-C_3N_4/NH_2-MIL-88B(Fe)	MB^+	30	Vis (500 W)	120	30	16
Cu_4I_4[Cu(5-eatz)$_2$]$_2$	MB^+	55	Vis (300 W)	300	50	17
Cu(I)(ptz)	MB^+ (H_2O_2)	18.7	Vis (500 W)	24	98	18
[Co(tib)$_2$]·SO_4	MB^+	10	Vis (300 W)	25	100	19
1	**MB^+**	**20**	**Vis (300 W)**	**20**	**99**	**This work**

References

1. Z. Wang, J. H. Zhang, J. J. Jiang, H. P. Wang, Z. W. Wei, X. J. Zhu, M. Pan and C. Y. Su, A stable metal cluster-metalloporphyrin MOF with high capacity for cationic dye removal, *J. Mater. Chem. A*, 2018, **6**, 17698-17705.
2. Z. Wang, C. Y. Zhu, H. S. Zhao, S. Y. Yin, S. J. Wang, J. H. Zhang, J. J. Jiang, M. Pan and C. Y. Su, Record high cationic dye separation performance for water sanitation using a neutral coordination framework, *J. Mater. Chem. A*, 2019, **7**, 4751-4758.
3. W. D. Fan, X. Wang, B. Xu, Y. T. Wang, D. D. Liu, M. Zhang, Y. Z. Shang, F. N. Dai, L. L. Zhang and D. F. Sun, Amino-functionalized MOFs with high physicochemical stability for efficient gas storage/separation, dye adsorption and catalytic performance, *J. Mater. Chem. A*, 2018, **6**, 24486-24495.
4. R. Issa, F. A. Ibrahim, M. Al-Ghoul and M. Hmadeh, Controlled growth and composition of multivariate metal-organic frameworks-199 via a reaction-diffusion process, *Nano Research*, 2021, **14**, 423-431.
5. Z. H. Xu, L. L. Han, G. L. Zhuang, J. Bai and D. Sun, In Situ Construction of Three Anion-Dependent Cu(I) Coordination Networks as Promising Heterogeneous Catalysts for Azide-Alkyne "Click" Reactions, *Inorg. Chem.*, 2015, **54**, 4737-4743.
6. J. Y. Wu, Y. Y. Gao, S. Wei, P. Chen, D. D. Gu, B. Fu and M. H. Chen, Plasma modification of Fe-MOF for efficient organic pollutants removal, *J. Solid State Chem.*, 2021, **302**, 9.
7. S. Q. Deng, Y. L. Miao, Y. L. Tan, H. N. Fang, Y. T. Li, X. J. Mo, S. L. Cai, J. Fan, W. G. Zhang and S. R. Zheng, An Anionic Nanotubular Metal-Organic Framework for High-Capacity Dye Adsorption and Dye Degradation in Darkness, *Inorg. Chem.*, 2019, **58**, 13979-13987.
8. Y. Rachuri, S. Subhagan, B. Parmar, K. K. Bisht and E. Suresh, Selective and reversible adsorption of cationic dyes by mixed ligand Zn(II) coordination polymers synthesized by reactant ratio modulation, *Dalton Trans.*, 2018, **47**, 898-908.
9. S. F. Jia, S. F. Song and X. D. Zhao, Selective adsorption and separation of dyes from aqueous solution by a zirconium-based porous framework material, *Appl. Organomet. Chem.*, 2021, **35**, 10.
10. S. H. Tian, S. Xu, J. T. Liu, C. He, Y. Xiong and P. Y. Feng, Highly efficient removal of both cationic and anionic dyes from wastewater with a water-stable and eco-friendly Fe-MOF via host-guest encapsulation, *J. Clean Prod.*, 2019, **239**, 10.
11. J. Guo, J. Yang, Y. Y. Liu and J. F. Ma, Two novel 3D metal-organic frameworks based on two tetrahedral ligands: syntheses, structures, photoluminescence and photocatalytic properties, *Crystengcomm*, 2012, **14**, 6609-6617.
12. J. J. Du, Y. P. Yuan, J. X. Sun, F. M. Peng, X. Jiang, L. G. Qiu, A. J. Xie, Y. H. Shen and J. F. Zhu, New photocatalysts based on MIL-53 metal-organic frameworks for the decolorization of methylene blue dye, *J. Hazard. Mater.*, 2011, **190**, 945-951.
13. C. F. Zhang, L. G. Qiu, F. Ke, Y. J. Zhu, Y. P. Yuan, G. S. Xu and X. Jiang, A novel magnetic recyclable photocatalyst based on a core-shell metal-organic framework Fe_3O_4@MIL-100(Fe) for the decolorization of methylene blue dye, *J. Mater. Chem. A*, 2013, **1**, 14329-14334.

14. H. Y. Sun, C. B. Liu, Y. Cong, M. H. Yu, H. Y. Bai and G. B. Che, New photocatalyst for the degradation of organic dyes based on $[Co_2(1,4\text{-BDC})(NCP)_2]_n\cdot 4nH_2O$, *Inorg. Chem. Commun.*, 2013, **35**, 130-134.
15. W. T. Xu, L. Ma, F. Ke, F. M. Peng, G. S. Xu, Y. H. Shen, J. F. Zhu, L. G. Qiu and Y. P. Yuan, Metal-organic frameworks MIL-88A hexagonal microrods as a new photocatalyst for efficient decolorization of methylene blue dye, *Dalton Trans.*, 2014, **43**, 3792-3798.
16. X. Y. Li, Y. H. Pi, L. Q. Wu, Q. B. Xia, J. L. Wu, Z. Li and J. Xiao, Facilitation of the visible light-induced Fenton-like excitation of H_2O_2 via heterojunction of g-C_3N_4/NH_2-Iron terephthalate metal-organic framework for MB degradation, *Appl. Catal. B-Environ.*, 2017, **202**, 653-663.
17. J. Liu, Y. H. Tang, F. Wang and J. Zhang, Syntheses of copper-iodine cluster-based frameworks for photocatalytic degradation of methylene blue, *Crystengcomm*, 2018, **20**, 1232-1236.
18. T. Wen, D. X. Zhang and J. Zhang, Two-Dimensional Copper(I) Coordination Polymer Materials as Photocatalysts for the Degradation of Organic Dyes, *Inorg. Chem.*, 2013, **52**, 12-14.
19. Q. G. Shang, T. Y. Zeng, K. Gao, N. N. Liu, Q. R. Cheng, G. Y. Liao, Z. Q. Pan and H. Zhou, A novel nitrogen heterocyclic ligand-based MOF: synthesis, characterization and photocatalytic properties, *New J. Chem.*, 2019, **43**, 16595-16603.